Code: github.com/sahu-lab/three-slab
More info: sahu-lab.github.io/pubs
Dated: 20 February 2026

Three-slab model for the dielectric permittivity of a lipid bilayer Supplemental Material

M.M.B. Sheraj [†,1] and Amaresh Sahu [‡,2]

[1] *Department of Physics, University of Texas, Austin TX 78712, USA*
[2] *McKetta Department of Chemical Engineering, University of Texas, Austin TX 78712, USA*

This document is the supplemental material (SM) to the manuscript of the same name. In §1, we determine how the three-slab model responds to both in-plane and out-of-plane electric fields, such that its parameters can be compared to molecular dynamics (MD) results. From here, simulation results for both dioleoylphosphatidylcholine (DOPC) and dipalmitoylphosphatidylcholine (DPPC) bilayers are presented in §2. Finally, the simulation methodology is provided in §3.

1. Analytical calculations: Three-slab response to electric fields

The three-slab model is shown in Fig. 2(a) of the main text. Here, we characterize the three-slab model at zero external field, determine how the model responds to in-plane and out-of-plane electric fields, and finally relate three-slab parameters to the results of molecular simulation.

1.1. Three-slab model at zero external field

To begin, we have a system comprised of linear dielectric slabs with bound surface charge densities σ_h at $z = \pm\delta_\mathrm{t}$ and $-\sigma_\mathrm{h}$ at $z = \pm(\delta_\mathrm{t}+\delta_\mathrm{h})$. When there is zero external electric field, the polarization density is given by $\langle P_z\rangle_0 = -\sigma_\mathrm{h}$ for $z \in (\delta_\mathrm{t}, \delta_\mathrm{t}+\delta_\mathrm{h})$, $\langle P_z\rangle_0 = \sigma_\mathrm{h}$ for $z \in (-\delta_\mathrm{t}-\delta_\mathrm{h}, -\delta_\mathrm{t})$, and $\langle P_z\rangle_0 = 0$ otherwise. In addition, since there is no free charge in the system, it is convenient to work with the electric displacement field $\langle \boldsymbol{D}\rangle_0 := \epsilon_0\langle \boldsymbol{E}\rangle_0 + \langle \boldsymbol{P}\rangle_0$. With the relation $\boldsymbol{\nabla}\cdot\langle \boldsymbol{D}\rangle_0 = 0$, translational and rotational invariance in the x–y plane, and mirror symmetry about $z = 0$, we find $\langle \boldsymbol{D}\rangle_0 = \boldsymbol{0}$ everywhere. By choosing $\langle\phi(\pm\ell/2)\rangle_0 = 0$ as our reference (recall $z \in [-\ell/2, \ell/2]$), it is straightforward to find

$$\langle\phi(z)\rangle_0 = \begin{cases} 0 & \delta_\mathrm{t}+\delta_\mathrm{h} < z < \ell/2 \\ \dfrac{\sigma_\mathrm{h}}{\epsilon_0}\left(\delta_\mathrm{t}+\delta_\mathrm{h}-z\right) & \delta_\mathrm{t} < z < \delta_\mathrm{t}+\delta_\mathrm{h} \\ \dfrac{\sigma_\mathrm{h}\delta_\mathrm{h}}{\epsilon_0} & -\delta_\mathrm{t} < z < \delta_\mathrm{t} \\ \dfrac{\sigma_\mathrm{h}}{\epsilon_0}\left(\delta_\mathrm{t}+\delta_\mathrm{h}+z\right) & -\delta_\mathrm{t}-\delta_\mathrm{h} < z < -\delta_\mathrm{t} \\ 0 & -\ell/2 < z < -\delta_\mathrm{t}-\delta_\mathrm{h}\ . \end{cases} \tag{1}$$

We thus confirm $\langle\phi(0)\rangle_0 - \langle\phi(\ell/2)\rangle_0 = \sigma_\mathrm{h}\delta_\mathrm{h}/\epsilon_0$, as presented in Eq. (7) of the main text.

[†] sheraj.physics@utexas.edu
[‡] asahu@che.utexas.edu

1.2. Response to in-plane electric fields

Let us consider, without loss of generality, an electric field that is imposed in the x-direction. At any given height z, a constant field $\hat{E}_x \boldsymbol{e}_x$ is applied via a potential difference $-\tilde{\ell}\hat{E}_x$ over a distance $\tilde{\ell}$ in the x-direction. The resultant polarization density is given by $\langle P_x \rangle_{\hat{E}_x} = 0$ in the tail region, $\langle P_x \rangle_{\hat{E}_x} = (\epsilon_{\mathrm{h}}^{\parallel} - \epsilon_0)\hat{E}_x$ in the head-group slab, and $\langle P_x \rangle_{\hat{E}_x} = (\epsilon_{\mathrm{w}} - \epsilon_0)\hat{E}_x$ in the surrounding water. We thus determine the integral of the in-plane polarization density over half of the system thickness to be

$$\int_0^{\ell/2} \big\langle P_x(z) \big\rangle_{\hat{E}_x} \, \mathrm{d}z \;=\; \int_0^{\ell/2} \Big(\epsilon_{\mathrm{slab}}^{\parallel}(z) - \epsilon_0 \Big) \hat{E}_x \, \mathrm{d}z \;=\; \hat{E}_x \left(\delta_{\mathrm{h}} (\epsilon_{\mathrm{h}}^{\parallel} - \epsilon_0) \,+\, \delta_{\mathrm{w}} (\epsilon_{\mathrm{w}} - \epsilon_0) \right) , \tag{2}$$

where $\epsilon_{\mathrm{slab}}^{\parallel}(z)$ is the spatially-dependent permittivity of the three-slab model. Recalling that $\hat{E}_x$ is constant and $\ell/2 = \delta_{\mathrm{t}} + \delta_{\mathrm{h}} + \delta_{\mathrm{w}}$, the final two expressions in Eq. (2) can be expressed as in Eq. (8) of the main text:

$$\int_0^{\ell/2} \epsilon^{\parallel}(z) \, \mathrm{d}z \;=\; \int_0^{\ell/2} \epsilon_{\mathrm{slab}}^{\parallel}(z) \, \mathrm{d}z \;=\; \delta_{\mathrm{t}} \epsilon_0 \,+\, \delta_{\mathrm{h}} \epsilon_{\mathrm{h}}^{\parallel} \,+\, \delta_{\mathrm{w}} \epsilon_{\mathrm{w}} \, . \tag{3}$$

1.3. Response to out-of-plane electric fields

In the absence of an electric field, the electric potential is symmetric and there is no potential drop across the system: $\langle \phi(\ell/2) \rangle_0 = \langle \phi(-\ell/2) \rangle_0 = 0$ (cf. §1.1). We now apply an out-of-plane electric field by imposing a potential drop $2\bar{\phi}$ over the distance ℓ, with $\langle \phi(\pm\ell/2) \rangle_{\hat{E}_z} = \mp\bar{\phi}$. To relate this potential drop to the field $\hat{E}_z \boldsymbol{e}_z$ applied in MD simulations, we recognize

$$2\bar{\phi} \;=\; \big\langle \phi(-\ell/2) \big\rangle_{\hat{E}_z} - \big\langle \phi(\ell/2) \big\rangle_{\hat{E}_z} \;=\; \big\langle \Delta\phi(-\ell/2) \big\rangle_{\hat{E}_z} - \big\langle \Delta\phi(\ell/2) \big\rangle_{\hat{E}_z} \;=\; \int_{-\ell/2}^{\ell/2} \big\langle \Delta E_z(z) \big\rangle_{\hat{E}_z} \mathrm{d}z \, . \tag{4}$$

By substituting Eq. (4) of the main text into Eq. (4) above and subsequently recognizing $\langle \Delta M_z \rangle$ is the integral of $\langle \Delta P_z(z) \rangle$ over the system volume, we find

$$2\bar{\phi} \;=\; \int_{-\ell/2}^{\ell/2} \left[\hat{E}_z + \frac{1}{\epsilon_0} \left(\frac{\langle \Delta M_z \rangle_{\hat{E}_z}}{V} - \big\langle \Delta P_z(z) \big\rangle_{\hat{E}_z} \right) \right] \mathrm{d}z \;=\; \hat{E}_z \ell \, , \qquad \text{such that} \qquad \bar{\phi} \;=\; \frac{\hat{E}_z \ell}{2} \, . \tag{5}$$

With the result of Eq. (5), we can compare analytical three-slab calculations with MD results.

We now determine the change in electric potential $\langle \Delta\phi(z) \rangle_{\hat{E}_z}$, electric field $\langle \Delta E_z(z) \rangle_{\hat{E}_z}$, and polarization density $\langle \Delta P_z(z) \rangle_{\hat{E}_z}$ upon establishing a potential drop with $\phi(\pm\ell/2) = \mp\hat{E}_z\ell/2$. To this end, we note that the system is translationally and rotationally invariant in the x–y plane, with no free charges—for which $\langle \boldsymbol{D} \rangle_{\hat{E}_z} = \langle D_z \rangle_{\hat{E}_z} \boldsymbol{e}_z$ with $\langle D_z \rangle_{\hat{E}_z}$ constant. Equating $\langle D_z \rangle_{\hat{E}_z}$ across the tail, head-group, and water layers yields

$$\epsilon_0 \big\langle E_{\mathrm{t}} \big\rangle_{\hat{E}_z} \;=\; \epsilon_{\mathrm{h}}^{\perp} \big\langle \Delta E_{\mathrm{h}} \big\rangle_{\hat{E}_z} \;=\; \epsilon_{\mathrm{w}} \big\langle E_{\mathrm{w}} \big\rangle_{\hat{E}_z} \, , \tag{6}$$

where $\langle E_{\mathrm{t}} \rangle_{\hat{E}_z}$ and $\langle E_{\mathrm{w}} \rangle_{\hat{E}_z}$ are the constant electric fields in the tail and water regions, and $\langle \Delta E_{\mathrm{h}} \rangle_{\hat{E}_z} := \langle E_{\mathrm{h}} \rangle_{\hat{E}_z} - \langle \Delta E_{\mathrm{h}} \rangle_0$ is the change in electric field in the head-group region (recall $\langle E_{\mathrm{t}} \rangle_0 = \langle E_{\mathrm{w}} \rangle_0 = 0$). Here $\epsilon_{\mathrm{h}}^{\perp}$ relates $\langle \Delta E_{\mathrm{h}} \rangle_{\hat{E}_z}$ to the change in head-group polarization density $\langle \Delta P_z \rangle_{\hat{E}_z}$ according to $\langle \Delta P_{\mathrm{h}} \rangle_{\hat{E}_z} = (\epsilon_{\mathrm{h}}^{\perp} - \epsilon_0) \langle \Delta E_{\mathrm{h}} \rangle_{\hat{E}_z}$. We then relate the change in the potential drop from $z = 0$ to $z = \ell/2$ to the integral of the change in electric field to find

$$\big\langle \Delta\phi(0) \big\rangle_{\hat{E}_z} - \big\langle \Delta\phi(\ell/2) \big\rangle_{\hat{E}_z} \;=\; \frac{\hat{E}_z \ell}{2} \;=\; \int_0^{\ell/2} \big\langle \Delta E_z \big\rangle_{\hat{E}_z} \mathrm{d}z \;=\; \delta_{\mathrm{t}} \big\langle E_{\mathrm{t}} \big\rangle_{\hat{E}_z} + \delta_{\mathrm{h}} \big\langle \Delta E_{\mathrm{h}} \big\rangle_{\hat{E}_z} + \delta_{\mathrm{w}} \big\langle E_{\mathrm{w}} \big\rangle_{\hat{E}_z} \, . \tag{7}$$

By combining Eqs. (6) and (7) and rearranging terms, we obtain

$$\epsilon_0 \langle E_\mathrm{t} \rangle_{\hat{E}_z} = \epsilon_\mathrm{h}^\perp \langle \Delta E_\mathrm{h} \rangle_{\hat{E}_z} = \epsilon_\mathrm{w} \langle E_\mathrm{w} \rangle_{\hat{E}_z} = \frac{\hat{E}_z \ell/2}{\delta_\mathrm{t}/\epsilon_0 + \delta_\mathrm{h}/\epsilon_\mathrm{h}^\perp + \delta_\mathrm{w}/\epsilon_\mathrm{w}} \,. \tag{8}$$

It is then straightforward to determine the change in electric potential, as plotted in Fig. 4(a) of the main text (for DPPC) and Fig. 1(f) here (for DOPC). In addition, the change in polarization density of the three-slab model can be written as

$$\langle \Delta P_z(z) \rangle_{\hat{E}_z} = \begin{cases} \dfrac{(\epsilon_\mathrm{w} - \epsilon_0)\, \hat{E}_z \ell/2}{\epsilon_\mathrm{w}(\delta_\mathrm{t}/\epsilon_0 + \delta_\mathrm{h}/\epsilon_\mathrm{h}^\perp + \delta_\mathrm{w}/\epsilon_\mathrm{w})} & z \in (-\ell/2, -\delta_\mathrm{t} - \delta_\mathrm{h}) \cup (\delta_\mathrm{t} + \delta_\mathrm{h}, \ell/2) \\ \dfrac{(\epsilon_\mathrm{h}^\perp - \epsilon_0)\, \hat{E}_z \ell/2}{\epsilon_\mathrm{h}^\perp(\delta_\mathrm{t}/\epsilon_0 + \delta_\mathrm{h}/\epsilon_\mathrm{h}^\perp + \delta_\mathrm{w}/\epsilon_\mathrm{w})} & z \in (-\delta_\mathrm{t} - \delta_\mathrm{h}, -\delta_\mathrm{t}) \cup (\delta_\mathrm{t}, \delta_\mathrm{t} + \delta_\mathrm{h}) \\ 0 & z \in (-\delta_\mathrm{t}, \delta_\mathrm{t}) \,. \end{cases} \tag{9}$$

With Eq. (9), we calculate the integral of $\langle \Delta P_z \rangle$ and $z\langle \Delta P_z \rangle$ from $z = 0$ to $z = \ell/2$, as provided in the right-hand sides of Eqs. (9) and (10) of the main text.

2. Additional MD simulation and three-slab results

The main text presents findings from MD simulations of a DPPC bilayer, and relates them to the three-slab model. In what follows, we repeat this analysis for a DOPC bilayer in §2.1. The success of the model in describing the electrostatics of another bilayer, at a different temperature, supports the generality of the three-slab construction. Additional DPPC results are provided in §2.2, and the calculation of the bulk water permittivity ϵ_w is described in §2.3.

2.1. The DOPC bilayer: Simulations and three-slab model

In contrast to DPPC bilayers, DOPC bilayers have a low melting temperature and so are in the fluid phase at room temperature. Here, we simulate a DOPC bilayer at 298.15 K and repeat the analysis described in the main text. The three-slab model is again successful in capturing zero-field behavior, as well as the membrane response to applied electric fields. All plots from Figs. 1–4 of the main text are reproduced for DOPC in Fig. 1 below.

2.2. The DPPC bilayer: Additional results

All plots in the main text correspond to a DPPC bilayer in the fluid phase at 323.15 K. In Fig. 2, we supplement this information with two additional plots. Figure 2(a) shows that the determination of $\epsilon^\parallel(z)$ via linear response and fluctuation formulas slightly disagrees when $\hat{E}^\parallel = 40$ mV/nm. We note that when this data was included in Fig. 3(a) of the main text, the resulting image was too cluttered and thus difficult to read. Figure 2(b) shows the average electric field $\langle E_z(z) \rangle$ in MD simulations and the three-slab model, for both $\hat{E}_z = 0$ and $\hat{E}_z = 70$ mV/nm. We notice that while the three-slab model captures only average features when $\hat{E}_z = 0$, the change in average field $\langle \Delta E_z(z) \rangle_{\hat{E}_z}$ is remarkably well-captured by the model.

2.2.1. Robustness of the model to different thickness definitions

As mentioned in the main text, there is not a single definition for the thickness δ_m of a lipid membrane in MD simulations. One common choice is to use the average distance between phosphorous

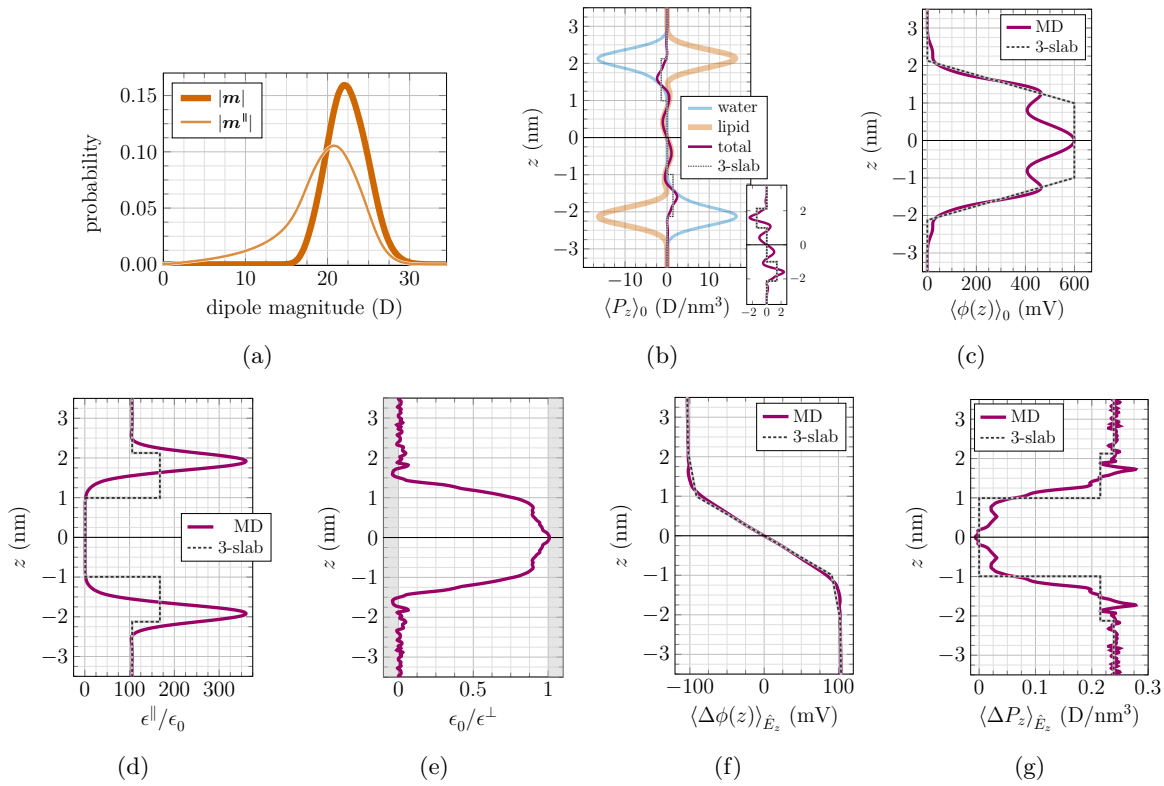

Figure 1: Results from MD simulations of a DOPC bilayer, and the corresponding three-slab model, following Figs. 1–4 of the main text. Note that in (f) and (g) here, $\hat{E}_z = 20$ mV/nm, and so the changes are smaller than their DPPC counterparts in the main text (where $\hat{E}_z = 70$ mV/nm). Despite quantitative differences between DOPC and DPPC data, the three-slab model successfully captures key features.

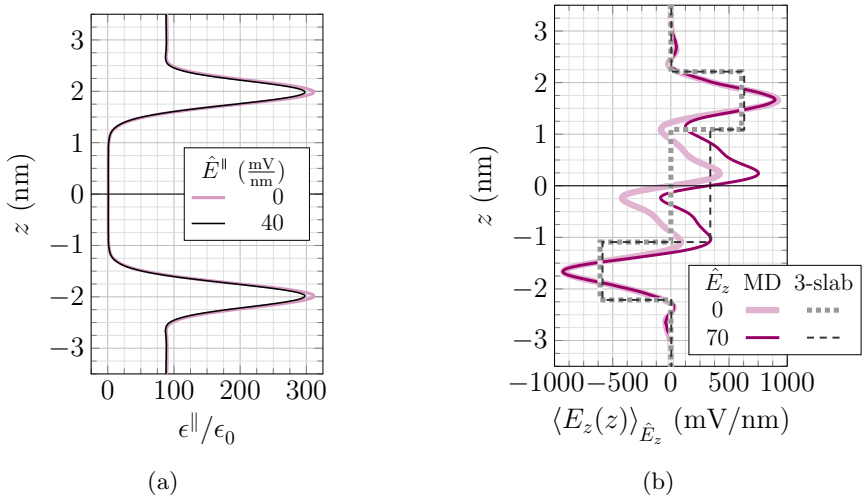

Figure 2: Additional results from MD simulations of a DPPC bilayer. (a) The in-plane permittivity $\epsilon^{\parallel}(z)$ is calculated from the zero-field fluctuation formula ($\hat{E}^{\parallel} = 0$) and the linear response formula (with $\hat{E}^{\parallel} = 40$ mV/nm). The two slightly differ in the head-group region, indicating that the response is weakly nonlinear when $\hat{E}^{\parallel} = 40$ mV/nm. Recall that the two formulas agreed for $\hat{E}^{\parallel} = 30$ mV/nm, as shown in Fig. 3(a) of the main text. (b) Calculation of the z-component of the average electric field $\langle E_z(z)\rangle_{\hat{E}_z} = -\langle \phi'(z)\rangle_{\hat{E}_z}$ for $\hat{E}_z = 0$ and 70 mV/nm, in both MD simulations and the three-slab model. The MD data predominantly shifts in the tail region, as does the three-slab prediction.

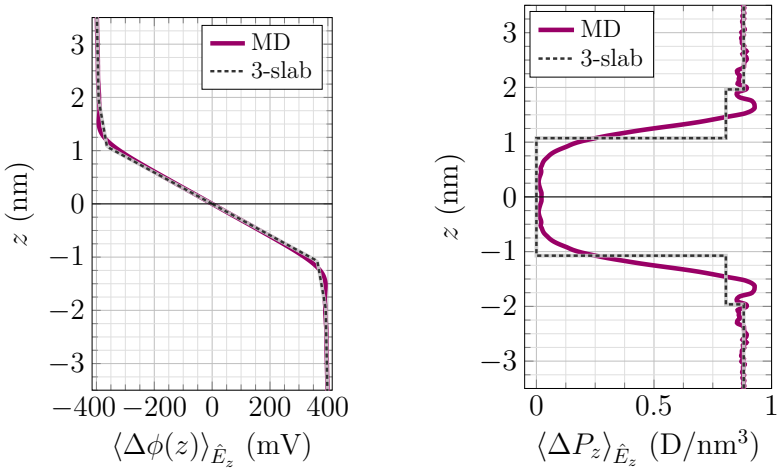

(a) (b)

Figure 3: Three-slab prediction of the change in electric potential (a) and z-component of the polarization density (b) of a DPPC bilayer upon application of an out-of-plane field $\hat{E}_z = 70$ mV/nm, after model parameters are calculated with data at $\hat{E}_z = 20$ mV/nm. Here, the membrane thickness is chosen as the average distance between phosphorous atoms in the top and bottom leaflets: $\delta_{\mathrm{m}}^{\mathrm{P-P}} = 3.9$ nm.

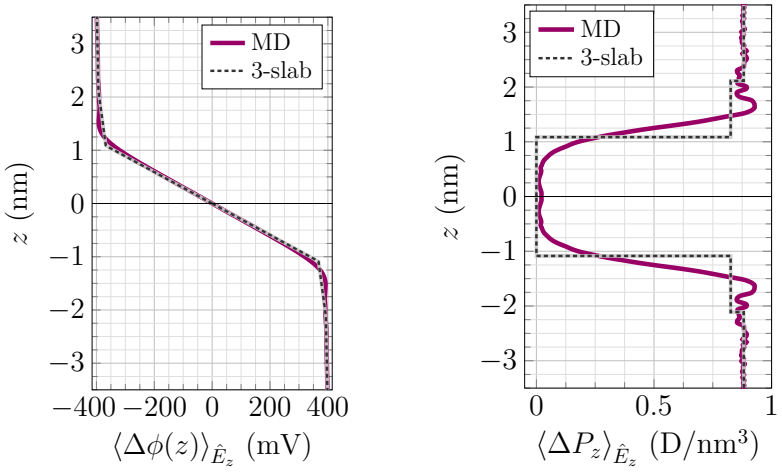

(a) (b)

Figure 4: Three-slab prediction of the change in electric potential (a) and z-component of the polarization density (b) of a DPPC bilayer upon application of an out-of-plane field $\hat{E}_z = 70$ mV/nm, after model parameters are calculated with data at $\hat{E}_z = 20$ mV/nm. Here, the membrane thickness is chosen as the average distance between nitrogen atoms in the top and bottom leaflets: $\delta_{\mathrm{m}}^{\mathrm{N-N}} = 4.2$ nm.

(P) atoms in the top and bottom leaflets; another approach is to use the average nitrogen–nitrogen (N–N) distance. In our simulations, we find $\delta_{\mathrm{m}}^{\mathrm{P–P}} = 3.9$ nm and $\delta_{\mathrm{m}}^{\mathrm{N–N}} = 4.2$ nm. For each choice of the membrane thickness, we calculate three-slab parameters using zero-field MD data and simulation results when $\hat{E}_z = 20$ mV/nm. Figures 3 and 4 display three-slab predictions at an applied field of $\hat{E}_z = 70$ mV/nm. As in the main text, we find that the model successfully predicts the change in electric potential and z-component of the polarization density.

Thus far, we verified that the three-slab model is successful for three different choices of the membrane thickness. For completeness, Fig. 5 shows that all model parameters vary smoothly over reasonable thickness values.

2.3. Calculation of the water permittivity

The bulk water permittivity ϵ_{w} enters the calculation of three-slab model parameters via Eqs. (2), (3), and (6)–(9) here, as well as Eqs. (9)–(11) in the main text. Here, we calculate ϵ_{w} at 298.15 K and 323.15 K, which are respectively the temperatures at which DOPC and DPPC simulations are run. Since the bulk water system is isotropic and homogeneous, $\langle \boldsymbol{P} \rangle_0 = \boldsymbol{0}$, $\langle \boldsymbol{M} \rangle_0 = \boldsymbol{0}$, $\langle \boldsymbol{M} \rangle_{\hat{\boldsymbol{E}}} = \langle \boldsymbol{P} \rangle_{\hat{\boldsymbol{E}}} V$, and (cf. Eqs. (2)–(4) of the main text)

$$\langle \boldsymbol{M} \rangle_{\hat{\boldsymbol{E}}} = \beta \Big(\langle \boldsymbol{M} \otimes \boldsymbol{M} \rangle_0 - \langle \boldsymbol{M} \rangle_0 \otimes \langle \boldsymbol{M} \rangle_0 \Big) \hat{\boldsymbol{E}} = (\epsilon - \epsilon_0) V \hat{\boldsymbol{E}} \, . \tag{10}$$

Since the field $\hat{\boldsymbol{E}}$ is arbitrary, the last equality in Eq. (10) requires

$$(\epsilon - \epsilon_0) V \boldsymbol{I} = \beta \Big(\langle \boldsymbol{M} \otimes \boldsymbol{M} \rangle_0 - \langle \boldsymbol{M} \rangle_0 \otimes \langle \boldsymbol{M} \rangle_0 \Big) \, . \tag{11}$$

Taking the trace of both sides of Eq. (11) and rearranging terms yields

$$\epsilon = \epsilon_0 + \frac{\beta}{3V} \Big(\langle \boldsymbol{M} \cdot \boldsymbol{M} \rangle_0 - \langle \boldsymbol{M} \rangle_0 \cdot \langle \boldsymbol{M} \rangle_0 \Big) \, , \tag{12}$$

which is the well-known fluctuation formula of a homogeneous, isotropic material [1, 2]. With Eq. (12), the permittivity of water can be calculated from MD simulations, with the ensemble average approximated by a time average. We plot the time average of five independent system replicas at a temperature of 323.15 K in Fig. 6, along with the average over replicas, to determine $\epsilon_{\mathrm{w}}/\epsilon_0 = 89.3$ (see §3.3 for simulation parameters). An identical procedure was carried out for MD simulations of water at 298.15 K, from which we determine $\epsilon_{\mathrm{w}}/\epsilon_0 = 106$.

3. Simulation methods

All MD simulations employ the CHARMM36m all-atom force field for lipids [3], and were carried out using the GROMACS 2024.2 software package [4, 5]. The lipid force fields are parametrized with the TIP3P water model [6], which is used throughout. Systems were generated using Version 3.7 of the CHARMM-GUI tool [7].

3.1. DPPC bilayer simulations

In DPPC bilayer simulations, the system consisted of 64 DPPC molecules—32 in each leaflet—and 5120 TIP3P water molecules. Initially, the simulation box had height $\ell = 12.292$ nm, and the area per lipid in the x–y plane was 0.63 nm^2. From this starting structure, 80 replicas were simulated by assigning different initial velocity distributions to each replica, and then applying the same equilibration protocol. Each replica was simulated in the canonical (NVT) ensemble for two

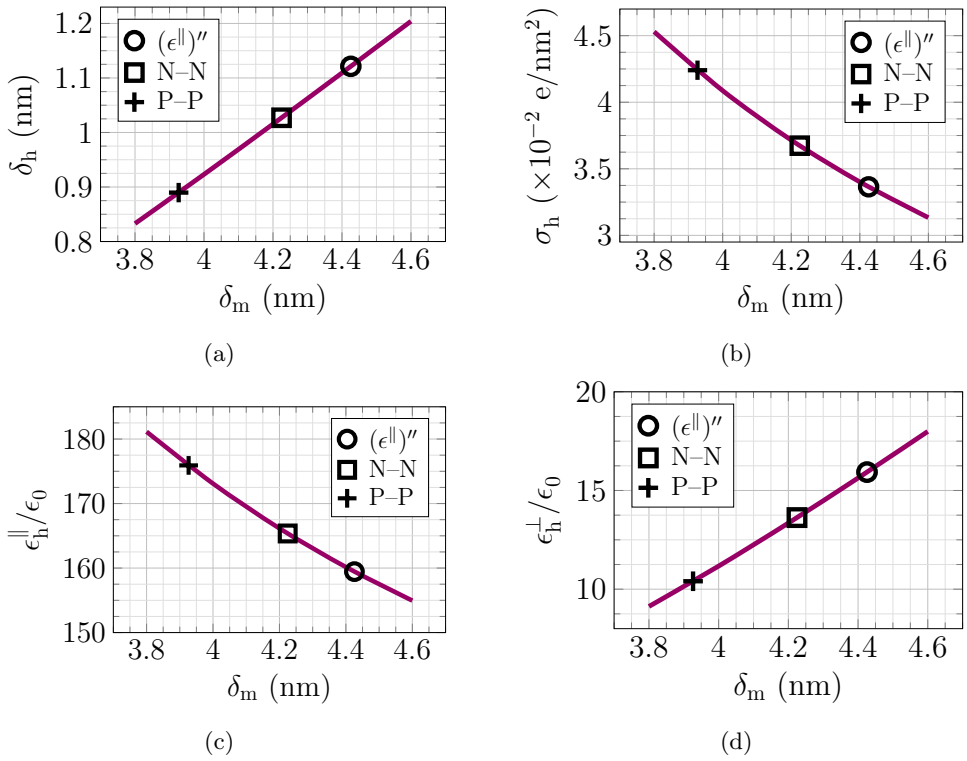

Figure 5: Three-slab model parameters as a function of the membrane thickness δ_m, which can be chosen arbitrarily. Circular symbols represent the choice of thickness used in the main text, namely twice the distance from the bilayer midplane to where $d^2\epsilon^{\parallel}/dz^2 = 0$ at the membrane–water interface. The nitrogen–nitrogen and phosphorous–phosphorous definitions of the membrane thickness are also shown as squares and 'plus' symbols, respectively. We find the parameters smoothly vary as a function of the membrane thickness, further demonstrating the robustness of the model.

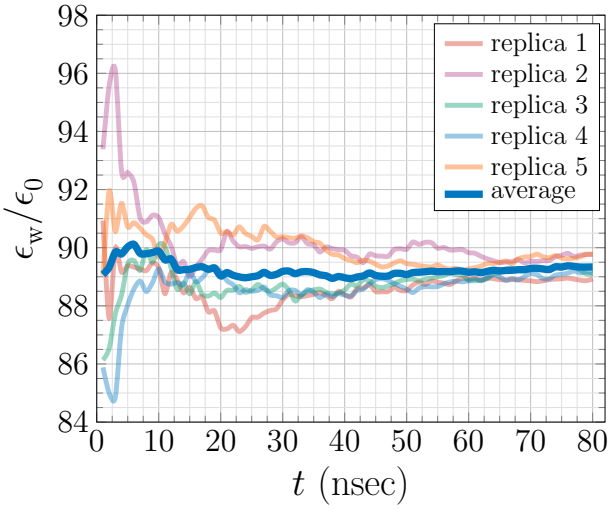

Figure 6: Calculation of the TIP3P water permittivity ϵ_w as a function of simulation time, for five replicas of the MD system, at temperature 323.15 K. We take the average value at the end of 80 nanoseconds to be the water permittivity used in three-slab calculations: $\epsilon_w/\epsilon_0 = 89.3$.

nanoseconds, followed by a four nanosecond simulation in the isothermal–isobaric (NPT) ensemble using the `c-rescale` barostat option, with a pressure of 1.0 bar. At this point, each of the 80 replicas had a different volume, and an additional 14 nanosecond NVT simulation was carried out for each.

From 80 equilibrated replicas, we calculated the average volume, and then chose the single replica with volume closest to the mean as our starting configuration. The other 79 replicas were not used any further. We generated a total of 40 replicas of the starting configuration; each was initialized with an independent velocity distribution. Twenty nanoseconds of NVT equilibration was carried out, followed by a 100 nanosecond NVT production run. There is accordingly a total of four microseconds of production data for our zero-field calculations, and the same protocol was used for a system subjected to an out-of-plane electric field. For simulations with an in-plane electric field, only five (rather than 40) replicas were used in the production simulations, as the data was found to converge more quickly.

The GROMACS script files are provided at the URL `github.com/sahu-lab/three-slab`. Each production trajectory was 100 nanoseconds long, with a two femtosecond time step (using the `md-integrator` option), sampled at one picosecond intervals. Periodic boundary conditions were employed, and the temperature was maintained at 323.15 K using the `v-rescale` thermostat option. In the NPT equilibration, the pressure was isotropic—for which the surface tension is zero. Long-range electrostatic interactions were treated with the particle-mesh Ewald method, along with conducting boundary conditions.

3.2. DOPC bilayer simulations

An identical protocol was used to simulate a DOPC bilayer. The system once again consisted of 64 lipid molecules and 5120 water molecules; the initial box had height $\ell = 11.586$ nm with an area per lipid of 0.697 nm^2. The temperature was maintained at 298.15 K throughout.

3.3. Bulk water simulations

The initial water system was a cube with side length 5.0 nm, containing 3916 TIP3P water molecules. From here, 60 replicas were assigned different starting velocity distributions, and equilibrated according to the protocol in §3.1. A starting configuration was then chosen, with volume closest to the average across replicas. From this single configuration, five replicas were generated, initialized with different velocity distributions, and equilibrated for 20 nanoseconds in the NVT ensemble. The production run consisted of 80 nanoseconds of NVT simulation for each replica. The entire water simulation protocol was carried out at both 298.15 K and 323.15 K.

References

[1] Kirkwood, J. G. The dielectric polarization of polar liquids. *J. Chem. Phys.* **7**, 911–919 (1939).

[2] Neumann, M. Dipole moment fluctuation formulas in computer simulations of polar systems. *Mol. Phys.* **50**, 841–858 (1983).

[3] Klauda, J. B. *et al.* Update of the CHARMM all-atom additive force field for lipids: Validation on six lipid types. *J. Phys. Chem. B* **114**, 7830–7843 (2010).

[4] Berendsen, H., van der Spoel, D. & van Drunen, R. GROMACS: A message-passing parallel molecular dynamics implementation. *Comp. Phys. Commun.* **91**, 43–56 (1995).

[5] Abraham, M. *et al.* GROMACS 2024.2 Manual (2024).

[6] Jorgensen, W. L., Chandrasekhar, J., Madura, J. D., Impey, R. W. & Klein, M. L. Comparison of simple potential functions for simulating liquid water. *J. Chem. Phys* **79**, 926–935 (1983).

[7] Feng, S., Park, S., Choi, Y. K. & Im, W. CHARMM-GUI membrane builder: Past, current, and future developments and applications. *J. Chem. Theory Comput.* **19**, 2161–2185 (2023).